

# Tradeoffs in the Design of a Spaceborne Scanning Pencil Beam Scatterometer: Application to SeaWinds

Michael W. Spencer, Chialin Wu  
Jet Propulsion Laboratory  
California Institute of Technology

David G. Long  
Electrical and Computer Engineering Dept.  
Brigham Young University

Sept 18, 1995

## Abstract

SeaWinds is a spaceborne windscatterometer to be flown on the second Japanese Advanced Earth Observing Satellite (ADEOS II) in 1999. An important international element of NASA's Earth Observing System (EOS), SeaWinds is an advanced follow-on to the NASA Scatterometer (NSCAT) on the first ADEOS platform. Unlike previous operational spaceborne scatterometer systems, SeaWinds employs a scanning "pencil-beam" antenna rather than a "fan-beam" antenna, making the instrument more compact and yielding greater ocean coverage. The goals of this paper are twofold. First, the overall SeaWinds functional design and backscatter measurement approach are described, and the relative advantages of the pencil-beam technique are outlined. Second, the unique aspects of measurement accuracy optimization and signal processing for the SeaWinds instrument are discussed. Applying the results (of a separate companion paper [1]), a technique to significantly improve measurement accuracy by modulating the transmit pulse is described. Trade-offs to optimize the transmit modulation bandwidth are presented.

## 1. Introduction

The SeaWinds scatterometer will be launched aboard the second Japanese Advanced Earth Observing Satellite (ADEOS II) in early 1999. SeaWinds, as part of the NASA Earth Observing System (EOS), will acquire all-weather measurements of ocean wind speed and direction. SeaWinds observations will continue the Ku-Band scatterometer data base begun

by NSCAT [14] into the next century. Because knowledge of near-surface winds over the ocean is critical for the investigation of many oceanographic and meteorological phenomena [3], SeaWinds observations form a key element of the EOS climatological research mission. In addition to its scientific applications, SeaWinds is expected to provide an important data source for operational meteorologists. Accurate, timely observations of ocean winds will enhance the ability of forecasters to identify coastal and marine hazards.

As with all scatterometers, SeaWinds will obtain an estimate of the wind by measuring the ocean surface radar backscatter cross section ( $\sigma^0$ ) at multiple azimuth angles. The geophysical model function, which relates wind speed and direction to backscatter cross section, is then numerically inverted to infer the near-surface wind. This technique has been successfully employed on previous scatterometer programs, such as Seasat andERS-1, and is planned for SeaWinds' direct predecessor, NSCAT [1, 5, 14]. Unlike these earlier scatterometers which employed a fixed "fan-beam" antenna, however, SeaWinds will utilize a scanning "pencil-beam" design.

In fan-beam systems, stick-like antennas are used to broadcast long, narrow radar footprints on the ocean surface. Along track  $\sigma^0$  resolution is defined by the 10% dimension of the footprint, and cross track resolution is obtained by either Doppler or range discrimination. Typically, a 500-600 km swath of measurements can be obtained on either side of the spacecraft, but in the region  $\pm 200$  km from the satellite nadir track, wind vectors cannot be measured due to the inappropriately low incidence angles. The existence of this "nadir gap," significantly limits ocean coverage. Fan-beam systems are also difficult to accommodate on spacecraft due to long antennas with their associated fields of view. Complicated antenna deployments are typically required.

Pencil-beam scatterometer systems were first described by Moore and others [13], with several variations proposed by Long [7, 9]. In contrast to fan-beam scatterometers, pencil-beam systems utilize a parabolic dish antenna which is mechanically spun to scan the ocean surface. This compact design is more readily accommodated on spacecraft without deployments. Because the antenna beam is conically scanned at a constant incidence angle, a wider, contiguous swath is possible. This greatly increases ocean coverage relative to fan-beam systems. The constant, relatively high incidence angles of the pencil-beam measurements also contribute to greater wind accuracy [3]. An associated advantage is that the

model function relating  $\sigma^0$  to wind velocity need be known only over the discrete incidence angles at which the measurements are made, rather than the broad range of incidence angles required by fan-beam systems. For these reasons, a pencil-beam architecture was chosen for SeaWinds.

In addition to the antenna concept, another important facet of the scatterometer design is the signal processing approach used to measure the backscattered signal and to estimate  $\sigma^0$ . Because the determination of ocean surface wind is a very sensitive function of the  $\sigma^0$  measurement accuracy, a key consideration in the processor design is the minimization of the  $\sigma^0$  error variance. Errors in the estimate of  $\sigma^0$  are due to the random effects of additive signal fading and thermal noise, as well as calibration uncertainty. In general,  $\sigma^0$  accuracy is improved by increasing the effective number of independent samples and the signal-to-noise ratio (SNR) associated with the measurement [2, 8]. Because  $\sigma^0$  is a function of wind speed backscatter cross section is low for low winds and high for high winds – the SNR can vary considerably as different wind conditions are observed.

The issues and trade-offs encountered in selecting an optimal signal processing approach are generally different for fan-beam systems and pencil-beam systems. With fan-beam systems,  $\sigma^0$  cell resolution is determined by either Doppler or range discrimination techniques, increasing overall processor complexity. Another challenge for fan-beam systems is that the antenna beam is very broad in one dimension, and the transmit energy is spread over a wide region. This may result in low SNR for the backscattered signal, particularly at low wind speeds. On the other hand, an advantage enjoyed by fan-beam systems is that, because the broad beam illuminates the entire swath simultaneously, relatively long integration times, and thus more independent samples, are possible.

Pencil-beam systems, by contrast, can use relatively simple processors because  $\sigma^0$  resolution is completely defined by the antenna beam dimensions. Because energy is focused on a small region, SNR is generally higher for pencil-beam systems. Pencil-beam systems, however, have considerably less integration time available as the antenna footprint is quickly scanned from one location to another. A key challenge for the SeaWinds signal processing design is how to optimize performance by improving the effective number of independent samples. It is demonstrated that appropriate use of transmit pulse modulation can accomplish this goal.

The main body of this paper is divided into two distinct parts. In Section II the overall SeaWinds system design and  $\sigma^0$  measurement approach are described. Included are brief descriptions of the instrument parameters, antenna scan approach, timing, and back scattered energy detection. Section III provides a more detailed look at the unique aspects of the Swin'ilds signal processing design, and discusses the trade-offs performed in order to achieve optimum  $\sigma^0$  measurement performance. In particular it is shown how pseudorandom phase modulation of the transmit pulse is employed to minimize  $\sigma^0$  estimation error. A companion paper [11], which provides a theoretical basis for this technique, is referred to extensively.

## 11. SeaWinds System 1 Design

In preparation for a 1999 launch, the SeaWinds system is in an advanced stage of development. The Swin'ilds instrument is being designed to meet the science requirements for wind retrieval [3], and to be consistent with the ADEOS-II orbit and accommodation constraints. In this section the *functional* aspects of the SeaWinds instrument design are presented. Included are brief descriptions of the selected radar parameters, antenna scan approach, timing, echo detection, and  $\sigma^0$  calculation. In addition to providing a reference for the overall SeaWinds measurement technique, this description provides important background material against which the detailed signal processing tradeoffs in Section III are discussed. Additional information on the planned hardware implementation and ground data system can be found in Wu et al. [18].

### Antenna Characteristics and Measurement Geometry

In order to determine the near surface wind, a scatterometer must obtain measurements of  $\sigma^0$  at multiple azimuth angles for the same point on the ocean surface [16]. As illustrated in Figures 1 and 2, SeaWinds accomplishes this using two conically scanned pencil beams. An approximately one meter diameter parabolic dish antenna with two offset feeds is used to create both the "inner" and the "outer" beams. The inner beam maintains an "off-nadir" angle of 40 degrees, and intercepts the ocean at a constant 46 degrees incidence angle. The outer beam has an off-nadir angle of 46 degrees with an incidence angle of 54 degrees.

The antenna is mechanically spun about the nadir axis to generate a conical scan. The scan azimuth angle is measured counter-clockwise with 0 degrees defined as the antenna pointing in the direction of the spacecraft motion. As the spacecraft moves in its orbit, the beams trace overlapping helical patterns on the Earth's surface. Each point within the inner 700 km of the swath is viewed from four different azimuth angles - twice by the outer beam looking forward then aft, and twice by the inner beam in the same fashion. In the outside edge of the swath, between cross track distances of 700 and 900 km, each point on the ocean is viewed twice by the outer beam only. The availability of four, rather than two, measurements over most of the total swath will enhance the ability of SeaWinds to unambiguously determine wind direction. Wind direction performance is further improved by using different polarizations for each beam [14]. The inner beam is horizontally polarized with respect to the ocean surface (the transmitted E-vector is parallel to the surface). The outer beam is vertically polarized.

Note that, unlike fan-beam systems, the azimuth angle "mix" of the  $\sigma^0$  measurements going into the wind retrieval is not constant, but varies from nadir out to the edge of the swath. Near nadir the forward and aft measurements are approximately 180 degrees apart, while at the extreme edge of the swath the azimuth angle between the measurements approaches 0 degrees. Thus the wind retrieval performance of SeaWinds is observed to vary as a function of the distance from the nadir track, in general being optimum when the azimuth differences of the measurements are near 90 degrees [18]. But because the  $\sigma^0$  measurements are obtained at a favorable high incidence angle over a continuous 1800 km swath, there is no distinct "nadir gap" where wind can not be retrieved. Such a wide swath will cover 90% of the ocean surface within 24 hours, an improvement over the NSCAT coverage of 77% in 24 hours.

The SeaWinds antenna rotation rate and measurement timing were chosen to obtain optimal sampling of the surface  $\sigma^0$  and to meet host spacecraft dynamics requirements. The antenna rotation rate of 18 rpm combined with the nominal transmitter pulse repetition frequency (PRF) of 92.5 Hz for each beam, produces a regular pattern of measurements on the surface. Figure 3 shows this pattern for two consecutive rotations of the outer beam. The group of measurements displayed in Figure 3 corresponds roughly to the rectangular region drawn in Figure 2. Each transmit pulse event will obtain one measurement of  $\sigma_0$ ,

depicted in Figure 3 as an ellipse whose dimensions are defined by the 3 dB contours of the antenna pattern projected on the surface. The “along, scan” spacing of the measurements is a function of the scan rate and PRF, and is 15 km for the inner beam and 19 km for the outer beam. The “along track” displacement of the measurements is determined by the satellite ground speed of 6.6 km/sec, and is 22 km for both beams. The footprint dimensions and spacing are consistent with the requirements to coregister the four azimuthal measurements, and to achieve near 50 km. wind measurement resolution [3, 6]. Key parameters for each antenna beam and their associated footprints are summarized in Table 1,

### Radar Electronics Functional Design

Figure 4 depicts the basic design of the SeaWinds radar electronics and shows the transmit, receive, and detector functions. Upon command from the timing controller, the transmitter, which consists of a modulated signal generator driving a traveling wavetube (TWT) amplifier, issues a 1.5 ms duration, 110 Watt Ku-Band pulse. For reasons explained in Section 1.1.1, the transmit pulse is MSK modulated to a bandwidth of approximately 40 kHz. The pulse is routed to either the inner or the outer beam and through a coaxial rotary joint to the spinning section of the antenna assembly. The echo return is likewise directed to the receiver where it is amplified, downconverted, and detected. A summary list of the key radar parameters is shown in Table 2.

Due to the motion of the satellite relative to the Earth, a Doppler shift of between “1500” kHz is imparted to the echo return signal, depending on the antenna scan position. When the antenna is pointing forward or behind relative to the spacecraft motion (see Figure 1), the Doppler shift is at a maximum or minimum. When the antenna is scanned perpendicular to the spacecraft ground-track, the shift is near zero. In the SeaWinds design, the Doppler shift is pre-compensated by tuning the transmit carrier frequency to  $13.402 \text{ GHz} - f_d$ , where  $f_d$  is the expected frequency shift to be imparted to the return signal. The compensation frequency is computed by the Sea Winds on-board processor using the measured antenna position, orbit location, spacecraft velocity, and Earth rotation. Pre-compensating the transmit pulse for Doppler shift produces an echo signal that always occurs at the same center frequency, simplifying the RF down conversion and detector electronics. Note that the Doppler frequency could have been equivalently compensated by a variable RF frequency

in the receiver, rather than a variable transmit frequency.

An important feature of any scatterometer system is the accurate calibration of the transmit power and receiver gain [15]. In the SeaWinds instrument design, these parameters are measured simultaneously by periodically injecting the transmit pulse, attenuated by a known amount, into the receiver. To avoid corruption by spurious leakage power during a “loop-back” calibration event, a high loss receive protect switch is enabled.

### Echo Energy Detection and $\sigma^0$ Estimation

The received signal at the detector consists of the return echo plus thermal noise. The thermal noise component is a combination of the instrument system noise and the Earth scene brightness temperature. In order to estimate  $\sigma^0$ , a measurement of the echo energy only is required. In scatterometer systems this is generally achieved by subtracting a separate measurement of the thermal noise floor—the “noise-only” measurement—from the “signal+noise” measurement [2, 16].

A description of specific echo detection strategies for pencil-beam scatterometers is given in the companion paper [11]. For SeaWinds, an approach where the signal+noise and “noise-only” energies are measured simultaneously was selected. (Note that with the simultaneous detection approach, the “noise-only” measurement actually contains the echo energy as well. The term “noise-only,” which is commonly used in scatterometry, is nonetheless retained here). As shown in Figure 5, the signal+noise and noise-only energies,  $C_{sn}$  and  $C'_{no}$ , are obtained by integrating the output of two separate filter operations. Figure 6 shows a representation of the echo spectrum, thermal noise spectrum, and the magnitude response of the filters. The signal+noise filter has a bandwidth  $B_s = 80$  kHz and is centered on the echo return which has a 3 dB bandwidth of approximately 40 kHz. The noise-only filter has a much wider pass-band,  $B_n = 1$  MHz, which overlaps the narrower signal+noise measurement band. The specific choice of filter bandwidths is based on measurement accuracy considerations, which is the subject of Section III.

Details of the transmit pulse and echo detection timing are shown in Figure 7. The rectangular transmit pulses occur every 5.4 ms and alternate between the inner and outer beam. Note that this produces a PRI of approximately 92.5 Hz on each beam individually and 185 Hz overall. Due to the finite dimensions of the antenna footprint, the echo return

“pulses” are not replicas of the transmit pulse but are dispersed in time and frequency. The dispersion in time spreads the echo by approximately 0.5 ms, and is depicted in Figure 7 by showing the echoes as trapezoids. The round trip flight times for the inner and outer pulses are 7.3 and 8.3 ms respectively, and thus each echo returns after the *succeeding* transmit pulse. The range gate interval during which both the signal+ noise and noise-only measurements are accumulated is centered on the expected time of the echo return. In order to measure the entire energy of the echo, the range gate has a length  $T_r = T_n = 2$  ms.

The values  $C_{sn}$  and  $C'_{no}$  for each return pulse are telemetered to the ground where the echo energy and, ultimately,  $\sigma^0$  are estimated. For the SeaWinds detection scheme, an expression for the echo energy estimate is obtained in a straightforward manner. Assuming a processor gain of unity, the expected values of  $C_{sn}$  and  $C'_{no}$  are written as

$$\mathcal{E}[C_{sn}] = \rho_E E_s + B_r T_r n_0 \quad (1)$$

$$\mathcal{E}[C'_{no}] = E_s + B_n T_n n_0 \quad (2)$$

where  $E_s$  is the expected energy in the echo return,  $n_0$  is the one-sided thermal noise power spectral density, and  $\rho_E$  is the fraction of the echo energy passed by the signal+ noise filter. In the ideal case where the entire echo spectrum is captured by the filter,  $\rho_E = 1$ . This is true of the noise-only filter. For the signal+ noise filter, however, a small portion of the total energy from the sidelobes of the echo spectrum will be lost. The parameter  $\rho_E$  is easily calculated by integrating the echo spectrum and filter response. (See Eq. (15) and associated discussion).

Solving Eq. (1) and (2) for  $E_s$ , we obtain the following expression for the estimated echo energy,  $\widehat{E}_s$ , given  $C_{sn}$  and  $C'_{no}$ :

$$\widehat{E}_s = C_{sn} \frac{B_n}{\rho_E(B_n - B_r)} - C'_{no} \frac{B_r}{\rho_E(B_n - B_r)}. \quad (3)$$

The well known scatterometer radar equation [Sec. 7, [16]] is then applied to estimate  $\sigma^0$ :

$$\widehat{\sigma}_0 = \frac{\widehat{E}_s}{X} \quad (4)$$

where

$$X = \frac{E_t \lambda^2 G_0^2 A_c}{(4\pi)^2 R^4} \quad (5)$$

Here,  $E_t$  is the total transmit pulse energy,  $\lambda$  is the transmit carrier frequency,  $G_0$  is the antenna pattern peak gain,  $A_c$  is the effective illuminated footprint area, and  $R$  is the nominal slant range. For this paper, which specifically addresses the SeaWinds case,  $A_c$  is defined as:

$$A_c = \frac{R^4}{G_0^2} \int_{r, \omega_d} \frac{G_t(r, \omega_d) G_r(r, \omega_d)}{r^4} A_r(r, \omega_d) dr d\omega_d \quad (6)$$

where  $G_t$  is the antenna pattern at the time of transmit,  $G_r$  is the antenna pattern at the time of echo return,  $r$  is the range to each surface element,  $A_r$  is the area of each surface element, and the integration is performed over range and Doppler on the surface. The transmit and receive antenna positions are specified separately in Eq. (6) because the antenna rotates approximately 0.8 degrees – a significant fraction of the beamwidth – during the pulse round trip flight. A precise formulation of the radar equation must take this offset into account [12].

### III. Transmit Modulation and Processor Parameter Tradeoffs

In this section we turn from a general overview of the SeaWinds instrument system to a more detailed discussion of a key design issue: the minimization of  $\sigma_0$  measurement error. Here, general expressions for measurement variance derived in [11] are applied to the specific SeaWinds case in order to select the optimum transmit modulation and processor filter parameters.

An examination of Eq. (4) reveals that the error in determining  $\sigma^0$  has two main components: the error associated with the estimate of  $E_s$ , and the error in the knowledge of the value of  $X$ . The process of measuring all the radar parameters which contribute to  $X$  is referred to as scatterometer *calibration*. Calibration errors are largely *systematic* in that they are either biases or can be reduced by careful characterization of the on-orbit variations in the instrument radiometric parameters. Techniques for scatterometer calibration are beyond the scope of this paper but are discussed in detail elsewhere [10, 15]. The error associated with the estimate of  $E_s$ , however, is *random* and places a fundamental constraint on the theoretical wind performance of the scatterometer. It is this error that we seek to minimize here.

A metric, widely used in scatterometry, for evaluating the  $E_s$  estimation error is the

“ $K_p$ ” parameter:

$$K_p[\widehat{V}_s] = \left( \frac{\sqrt{\text{var}[\widehat{V}_s]}}{V_s} \right) \quad (7)$$

$K_p$  is the normalized standard deviation of  $\widehat{V}_s$  due to radar fading and thermal noise effects. A general objective of scatterometer design is the minimization of  $K_p$  [14]. In performing design tradeoffs, it is useful to have a “rule of thumb” maximum value of  $K_p$  to be achieved. Unfortunately,  $K_p$  is a function of the signal to noise ratio which depends on the wind. Further, relating  $K_p$  directly to the wind measurement performance can be difficult due to the non-linearity in the wind retrieval process. As a result, we adopt the goal for SeaWinds that  $K_p$  should be less than the geophysical modeling error – the percentage variation in  $\sigma^0$  for a given wind velocity [10]. Such a criterion will insure that wind performance is limited not by the precision of the instrument, but only by our ability to relate the measured  $\sigma^0$ 's to wind speed and direction via the model function. The magnitude of the geophysical modeling error at Ku-band is not well known, but a value of 17% has been commonly used in other scatterometer performance analyses. For SeaWinds a design goal is thus to have  $K_p < 0.17$ .

In the companion paper [11], the  $K_p$  expression for a pencil-beam scatterometer is derived, and has the generalized form:

$$K_p[\widehat{V}_s] = (A + SB + S^2C)^{\frac{1}{2}} \quad (8)$$

Where  $A$ ,  $B$ , and  $C$  are rather complex functions of the transmit modulation, range and Doppler characteristics of the illuminated footprint, and the echo and noise filter bandwidths.  $S$  is the noise-to-signal ratio ( $1/\text{SNR}$ ) within the signal+noise filter band, and is defined as

$$S = \frac{B_r T_r n_0}{V_s} \quad (9)$$

where  $V_s$ ,  $B_r$ ,  $T_r$ , and  $n_0$  are all as defined in the previous section. It is demonstrated in [11] that the “ $A$ ” term in Eq. (8), which is related to the effective number of independent samples, can be significantly decreased by appropriate modulation of the transmit pulse, thus decreasing  $K_p$ . A trade-off exists, however, because as the transmit pulse bandwidth increases, the bandwidth of the echo return necessarily increases and  $B_r$  must subsequently widen to accommodate the larger echo bandwidth. A larger  $B_r$  produces a larger  $S$  via Eq.

(9) which in turn tends to *increase*  $K_p$ . The objective here is to identify the modulation and filtering strategy which balances these effects and optimizes  $K_p$  for SeaWinds. Our approach will be to first define the modulation scheme and the transmit pulse bandwidth, calculate the resulting echo return bandwidth and the  $B_r$  required to accommodate it, and finally to evaluate Eq. (8) for the expected range of  $S$  in order to select the optimal modulation bandwidth and filter parameters.

### Modulation Format and Transmit Pulse Spectrum

As discussed in [11], modulation schemes which produce a “thumb-tack” shaped radar ambiguity function are good candidates for improving  $K_p$ . Due to its broad main lobe and low side lobe properties, as well as ease of implementation in hardware, a pseudorandom MSK (minimum phase shift keying) modulation format was selected for use with SeaWinds. Although all analysis in this paper is presented for the MSK case, similar techniques could be applied for other suitable modulation schemes (FSK, FSK, etc.).

When the transmit pulse length is much greater than the MSK modulation bit period, the one-sided energy spectral density,  $S_{msk}(\omega)$ , of the transmitted signal can be shown to be [4]:

$$S_{msk}(\omega) = 16\pi^2 E_t T_b \left[ \frac{\cos T_b(\omega - \omega_c - \omega_d) \frac{1}{2} \omega_d}{4T_b^2(\omega - \omega_c - \omega_d)^2 - \pi^2} \right]^2 \quad (10)$$

where  $E_t$  is the total energy in the transmit pulse,  $T_b$  is the modulation bit period,  $\omega_c$  is the angular frequency of the transmit carrier ( $2\pi \times 13.402$  GHz), and  $\omega_d$  is the doppler pre-compensation applied to the transmit pulse ( $2\pi \times f_d$ ). Note that the transmitted signal spectrum is centered at  $\omega_c - \omega_d$ . From Eq. (10) it can be shown that the 3 dB bandwidth of the transmit pulse,  $B_{msk}$ , is approximately given by

$$B_{msk} = \frac{0.6}{T_b}. \quad (11)$$

### Echo Return Spectrum

The spectrum of the echo return is different from that of the transmit pulse. The spectrum of the echo is a result of the interaction of the transmit signal with the ocean surface over the illuminated footprint. A well known technique for computing the echo return is to assume that the ocean surface is a collection of point scatterers (Sex. 7, [10]). The echo

return is a summation of replicas of the transmit pulse scattered from each point on the surface, suitably weighted by the antenna pattern at each scattering element, and frequency shifted by the Doppler associated with each scatterer. The echo energy spectrum is likewise a summation of replicas of the transmit energy spectrum weighted by the antenna pattern and shifted by the Doppler frequency. Thus, the expected one-sided echo return spectrum at the receiver input,  $E'(\omega)$ , can be written as a frequency domain convolution of the transmit spectrum and the footprint Doppler spectrum,  $D(\omega)$ :

$$E'(\omega) = S_{msk}(\omega) * D(\omega) \quad (12)$$

The Doppler spectrum represents the degree to which the transmit signal is spread in frequency due to the Doppler shift encountered over the illuminated area. Assuming a constant  $\sigma^0$  over the illuminated footprint, the Doppler spectrum,  $D(\omega)$ , is defined as

$$D(\omega) = \frac{\sigma^0 \lambda^2}{(4\pi)^3} \int \frac{G_t(r, \omega) G_r(r, \omega)}{r(r, \omega)^4} A_r(r, \omega) dr \quad (13)$$

where the integration is performed over the iso-range lines within the footprint (see the treatment in [11]). Note that the Doppler spectrum is centered at  $\omega_d$ , and consequently  $E'(\omega)$  is centered at WC. The downconverted, baseband echo spectrum incident on the detector,  $E(\omega)$ , is nominally centered at 0 Hz and is given by

$$E(\omega) = E'(\omega + \omega_c) \quad (14)$$

The shape and bandwidth of the Doppler spectrum, and thus the shape and bandwidth of the echo spectrum, depends on the selected antenna beam and azimuth angle. For SeaWinds, the 3 dB bandwidth of the Doppler spectrum,  $B_{dop}$ , varies from about 9 kHz, for the outer beam scanned in the forward or aft direction (0 or 180 degrees azimuth), to 15 kHz, for the inner beam scanned to the side (90 or 270 degrees azimuth).

Figure 8 is a graphical example of how the echo spectrum is calculated. Here, the transmit spectrum was computed from Eq. (10) assuming  $B_{msk} = 40$  kHz. The Doppler spectrum shown was produced by numerically evaluating Eq. (13) for the inner beam scanned to 90 degrees azimuth, and then removing the Doppler center frequency. The resulting baseband echo spectrum was computed from Eq. (12). All spectra were normalized to a peak value of unity. Note that for the case shown, and indeed in all cases where  $B_{msk} > B_{dop}$ , the transmit spectrum is the dominant factor in determining the bandwidth of the echo return.

## Signal+Noise and Noise-Only Filter Bandwidths

The signal+noise filter bandwidth,  $B_r$ , must be sufficiently wide to accommodate the echo return spectrum, yet as narrow as possible to minimize the amount of thermal noise passed. In the SeaWinds design process, two metrics are employed to assess the performance of the signal+noise filter: the fraction of the echo energy passed by the filter, and the Doppler compensation error. The fraction of the echo energy passed,  $\rho_E$ , is

$$\rho_E = \frac{\int |H_r(\omega)|^2 E(\omega) d\omega}{\int E(\omega) d\omega} \quad (15)$$

where  $|H_r(\omega)|^2$  is the magnitude response of the signal+noise filter, which is centered at 0 Hz. The Doppler compensation error is caused by inexact pre-compensation of the transmit carrier for echo Doppler shift. Nominally, the Doppler shift imparted to the return signal is perfectly pre-compensated and the echo spectrum is centered in the signal+noise filter. In reality, antenna position uncertainty and spacecraft attitude uncertainty lead to errors in Doppler tracking. The resultant error in detecting the echo energy,  $\Delta_E$ , is given by

$$\Delta_E = \int |H_r(\omega)|^2 E(\omega) d\omega - \int |H_r(\omega)|^2 E(\omega - \omega_{err}) d\omega \quad (16)$$

where  $\omega_{err}$  is the error associated with an inexact nulling of the Doppler center frequency, leading to an offset in the baseband echo spectrum. The filter bandwidth must be sufficiently wide to accommodate this “jitter” in the echo center frequency, without producing excessive error.

In examining the performance of the signal+noise filter, we shall define “filter overhead” as  $B_r - B_{msk}$ , or the additional bandwidth of the filter over the 3 dB bandwidth of the transmit pulse. In Figures 9a and 9b,  $\rho_E$  and  $\Delta_E$  are calculated for five different values of  $B_{msk}$  as a function of filter overhead. In evaluating Eq. (15) and Eq. (16),  $E(\omega)$  is computed with the  $D(\omega)$  that results from the inner beam scanned to 90 degrees azimuth, maximizing the frequency dispersion due to Doppler. Note that in the case of  $B_{msk} = 0$  kHz, the transmit signal is the unmodulated carrier and the echo spectrum is the same as the Doppler spectrum. The filter magnitude response is a 5th order Butterworth, an example of which for  $B_r = 80$  kHz is shown in Figure 8. In computing  $\Delta_E$ , the Doppler compensation error was fixed at 10 kHz ( $\omega_{err} = 2\pi \times 10^4$  rad/sec), the anticipated maximum value for the SeaWinds design.

From Figures 9a and 9b, we can determine a relationship between the transmitted  $B_{msk}$  and the required  $B_r$ . To insure that a sufficient fraction of the echo energy is passed, we require that the filter be wide enough to pass 90% of the echo energy. To minimize frequency jitter induced errors in the measurement of echo return energy, we require  $\Delta_F$  to be  $< 0.15$  dB. Applying these criteria to Figures 9a and 9b, we see that they are satisfied for a filter overhead of between 30 kHz and 50 kHz, depending on which  $B_{msk}$  is examined; the Doppler induced error being the primary factor for low values of  $B_{msk}$  and the percentage energy requirement being more important for large values of  $B_{msk}$ . In our trade-off analyses to find the optimum modulation bandwidth, we will find it useful to have a generalized relationship between  $B_{msk}$  and  $B_r$ . Such a relationship may be given by:

$$B_r = B_{msk} + 40kHz. \quad (17)$$

Thus, we will size: the bandwidth of the signal+noise filter to be 40 kHz larger than the 3 dB bandwidth of the transmit pulse spectrum.

The role of the noise-only filter is to provide a separate measurement so that the thermal noise component can be subtracted from the signal+noise. As shown in the companion paper [11], the contribution to  $K_p$  due to the noise-only measurement is minimized for  $B_n \gg B_r$ . For the range of  $B_{msk}$  and  $B_r$  considered in the SeaWinds trade-off analyses -  $B_{msk} = 0$  to 160 kHz,  $B_r = 40$  to 200 kHz - a noise-only filter bandwidth of  $B_n \geq 1$  MHz will meet this condition. In general, however, the precise selection of the noise-only filter parameters is a less critical one than the selection of the signal+noise filter parameters.

### Selection of $B_{msk}$ for $K_p$ Optimization

Having specified the gate times  $T_r$  and  $T_n$ , the modulation format, the required  $B_r$  given  $B_{msk}$ , and the required  $B_n$ ; we can now evaluate Eq. (8) and address our primary goal of choosing the  $B_{msk}$  which optimizes  $K_p$ . The parameters  $A$ ,  $B$ , and  $C$  are computed numerically as a function of antenna scan angle from the appropriate equations in the companion paper [11]. The correlation and cross-correlation integrals involved in the calculation of  $A$  and  $B$  are performed using the SeaWinds geometry and antenna patterns. The modulation function,  $a(t)$ , is generated using a maximal length, pseudo-random sequence which produces a  $B_{msk}$  consistent with Eq. (11). Because  $K_p$  is calculated for a single pulse,  $N_p = 1$ .

As an example, Figure 10 shows  $A$ ,  $B$ , and  $C$  as a function of azimuth for  $B_{msk} = 40$  kHz,  $B_r = 80$  kHz, and  $B_n = 1$  MHz. Note how, consistent with the observations in [11], the “ $A$ ” term varies significantly with azimuth.

Noise-to-signal ratio,  $S$ , is an equally important consideration in the trade-off analysis. To insure that  $K_p$  is optimized over the full range of possible ocean wind conditions,  $S$  is calculated from Eq. (9) for three representative echo return energies corresponding to low wind (3 m/s), moderate wind (8 m/s), and high wind (20 m/s) speed. These echo return strengths are shown in Table 3, and were computed using the nominal SeaWinds instrument parameters and the average  $\sigma^0$  as taken from the “SASS-2” model function [17]. The values of  $P_s$  are given in dBJoules at the input to the SeaWinds receiver. The thermal noise power spectral density,  $n_0$ , is assumed to be -200 dBW/Hz.

In Figures 11a, 11b, and 11c,  $K_p$  vs. azimuth angle for a range of  $B_{msk}$  is plotted for each beam at the three representative wind speeds. Because the effects of modulation are nearly symmetric with azimuth quadrant, only the azimuth range between 0 and 90 degrees is shown. Note that transmit modulation significantly reduces  $K_p$  for most of the swath, but offers little improvement for scan angles pointed forward or aft of the spacecraft - near 0 and 180 degrees. The curves also exhibit an important trend as a function of wind speed. At the high wind speeds where  $S$  is small, the “ $A$ ” term in Eq. (8) dominates and a larger  $B_{msk}$  leads to lower  $K_p$ . Thus, in a high SNR environment, measurement accuracy can be improved by modulating the signal and consequently increasing the effective number of independent samples. At lower wind speeds, however,  $K_p$  can actually increase for larger  $B_{msk}$ . This is particularly evident for the inner beam case in Figure 11a. Here, the benefit derived from modulating the signal is overcome by the deleterious effect of increasing  $B_r$  and passing more thermal noise to the detector.

An evaluation of the curves in Figure 11 led to the selection of  $B_{msk} = 40$  kHz and  $B_r = 80$  kHz for SeaWinds. Relative to the unmodulated case,  $B_{msk} = 40$  kHz significantly improves  $K_p$  performance over most of the swath and for most wind conditions. Lower values of  $B_{msk}$  produced inferior performance at high and moderate wind speeds, in general failing to meet the performance goal of  $K_p < 0.17$ . Higher values of  $B_{msk}$  were judged to produce undesirably large  $K_p$  at low speeds. Due to the greater scientific importance of high wind measurements, a degree of performance degradation at low wind speeds, such as

that experienced with  $B_{mask} = 40$  kHz for the inner beam at 3 m/s, was deemed acceptable. Note that for the values of  $S$  achievable with the SeaWinds design parameters, the goal of  $K_p < 0.17$  is not possible at the very lowest wind speeds for any modulation bandwidth. Despite being “ $K_p$  limited” rather than “model function limited” in the less critical low wind speed regime, SeaWinds performance simulations indicate that the desired measurement accuracies will still be met [18].

### Simultaneous vs. Non-Simultaneous Detection

As discussed in [11], the determination of  $B_s$  can be made with either of two different detection schemes, (1) signal+noise energy and noise-only energy are measured at the same time and in the same band (termed “simultaneous” detection), or (2) echo and noise energy are measured at different times or in different bands (“non-simultaneous” detection). In the case of non-simultaneous detection, the echo and noise measurements are independent, in the overlapping case they are not.

The minimum  $K_p$  is achieved for non-simultaneous detection. For SeaWinds, however, there are distinct advantages to using simultaneous detection. Because the antenna is scanning, the scene brightness temperature, which contributes to the noise floor we are attempting to subtract out, may change quickly (see Figure 3). This will be particularly true near ocean/land or ocean/ice boundaries. Thus, a simultaneous measurement of the noise energy will eliminate potential biases due to spatial mislocation with respect to the echo measurement. An additional reason to desire simultaneous detection is to simplify the hardware; the timing and IF frequencies are the same for the two measurements.

To assess the degree of degradation in  $K_p$  suffered by using a simultaneous detection scheme,  $K_p$  for the simultaneous and non-simultaneous cases were compared for the selected SeaWinds modulation and filter parameters. It was found that the percentage  $K_p$  increase due to using the simultaneous scheme was less than 3%—an acceptable amount. This is due to the fact that, as pointed out in [11],  $K_p$  for the simultaneous case approaches that of the non-simultaneous case when  $B_n \gg B_r$ . This is true for SeaWinds as  $B_n \geq 1$  MHz and  $B_r = 80$  kHz.

## 1 V. Summary

The functional design and relative advantages of the SeaWinds scatterometer have been described. Because SeaWinds employs a compact dish antenna rather than multiple fan-beam antennas, the instrument is more easily accommodated on spacecraft than previously flown scatterometers. The SeaWinds swath is 1800 km wide and will allow global ocean surface winds to be measured more frequently.

It was demonstrated how SeaWinds  $\sigma^0$  measurement variance is minimized by employing MSK modulation of the transmit pulse. For the SeaWinds system there is a trade-off between performance at higher wind speeds, which is enhanced by modulation, and performance at lower wind speeds, which may be degraded by modulation. The selected modulation and filter parameters -  $B_{msk} = 40$  kHz,  $B_r = 80$  kHz,  $B_n \geq 1$  MHz - insure that measurements at moderate and high wind speeds are significantly improved, whereas only slight degradation occurs at low wind speeds. At high wind speeds, which are of intense scientific interest,  $\sigma^0$  measurement accuracy is improved by 40% over the no-modulation case. This improved  $\sigma^0$  measurement accuracy will bring about a corresponding improvement in wind retrieval accuracy.

Due to the inherent advantages of the pencil-beam approach, future scatterometer systems which follow SeaWinds are likely to use a similar architecture. Although we have concentrated on the specific SeaWinds design, it is hoped that the design issues and trade-offs discussed will be of general utility for other spaceborne scatterometers.

## References

- [1] E.P.W. Attema, "The Active Microwave Instrument On-Board the ERS-1 Satellite," *Proceedings of the IEEE*, pp. 791-799, Vol. 79, No. 6, June 1991.
- [2] R. Fisher, "Standard Deviation of Scatterometer Measurements From Space," *IEEE Trans. Geosci. Electron.*, Vol. GE-10, No. 2, April 1972.
- [3] M.H. Freilich, D.G. Long, and M.W. Spencer, "SeaWinds: A Scanning Scatterometer for ADEOS 11 - Science Overview," *Proceedings of the International Geoscience and Remote Sensing Symposium*, Pasadena, California, August 8-12, pp. 960-963, 1994.
- [4] S. Haykin, *Communication Systems*, 2nd edition, John Wiley & Sons, New York: New York, 1983.
- [5] W.L. Jones, L.C. Schroeder, D.H. Boggs, E.M. Bracalente, R.A. Brown, G.J. Dome, W.J. Pierson, and F.J. Wentz, "The SEASAT-A Satellite Scatterometer: The Geophysical Evaluation of Remotely Sensed Wind Vectors Over the Ocean," *Journal of Geophysical Research*, Volume 87, Number C5, April 30, 1982.
- [6] D.G. Long, "Wind Measurement Resolution for a Scanning Pencil Beam Scatterometer," *Proceedings of the International Geoscience and Remote Sensing Symposium*, Pasadena, California, August 8-12, pp. 948-952, 1994.
- [7] D.G. Long, "ASCALJ: A Light-Weight, Low-Cost Scatterometer," in *Microwave Instrumentation for Remote Sensing of the Earth*, James C. Shiue, d., *Proc. SPIE 1935*, pp. 28-38, Orlando, Florida, April 13-14, 1993.
- [8] D. Cj. Ijollg, C-ITClli, atcl I:1{. Iii, "The Design of an Onboard Digital Doppler Processor for a Spaceborne Scatterometer," *IEEE Trans. Geoscience and Remote Sensing*, Vol. 26, No. 6, pp 869-878, Nov. 1988.
- [9] D.G. Long, M.H. Freilich, D. F. Leotta, and D.E. Noon, "A Scanning Scatterometer for the Eos Polar Platform," *Proceedings Of the International Geoscience and Remote Sensing Symposium*, pp. 2447-2450, Washington, D.C., May 20-24, 1990.

- [10] D.G. Long and G.B. Skouson, "Calibration of Spaceborne Scatterometers Using Tropical Rainforests," *IEEE Trans. Geoscience and Remote Sensing*, March, 1996.
- [11] D.G. Long and M.W. Spencer, "Radar Backscatter Measurement Accuracy for a Spaceborne Pencil-Beam Wind Scatterometer with Transmit Modulation," submitted to *IEEE Trans. Geoscience and Remote Sensing*, 1995.
- [12] R.K. Moore, "Effect of Pointing Errors and Range on Performance of Dual-Pencil-Beam Scatterometers," *IEEE Trans. Geoscience and Remote Sensing*, Vol. 23, No. 6, pp 901-905, November 1985.
- [13] R.K. Moore, R.G. Kennett, and F.K. Li, "Performance of a Scanning Pencil-Beam Spaceborne Scatterometer for Ocean Wind Measurements," *Proceedings of the International Geoscience and Remote Sensing Symposium*, pp. 563-564, Edinburgh, Scotland, Aug. 1988.
- [14] F. Naderi, M.H. Freilich, and D.G. Long, "Spaceborne Radar Measurement of Wind Velocity Over the Ocean- An Overview of the NSCAT Scatterometer System," *Proceedings of the IEEE*, pp. 850-866, Vol. 79, No.6, June 1991.
- [15] M.W. Spencer, W. Tsai, S. Yuel, and G. Neumann, "NASA Scatterometer Calibration Philosophy and Approach," in *Microwave Instrumentation for Remote Sensing Of the Earth*, James C. Shiue, ed., *Proc. SPIE 1935*, pp. 63-73, Orlando, Florida, April 13-14, 1993.
- [16] F.T. Ulaby, R.K. Moore, and A.K. Fung, *Microwave Remote Sensing - Active and Passive*, Reading, Mass: Addison-Wesley Publishing Company, 1981.
- [17] F.J. Wentz, S. Petcherych, and L.A. Thomas, "A Model Function for Ocean Radar Cross Sections at 14.6 GHz," *J. Geophysical Res.*, Vol 89, pp. 3681-3704, 1984.
- [18] C. Wu, J. Graf, M. Freilich, D.G. Long, M. Spencer, W. Tsai, D. Lisman, and C. Wilm, "The SeaWinds Scatterometer Instrument," *Proceedings of the International Geoscience and Remote Sensing Symposium*, Pasadena, California, August 8-12, pp. 1511-1515, 1994.

## Tables

Parameter	Inner Beam	Outer Beam
Polarization	H	V
Elevation Angle	40°	46°
Surface Incidence Angle	47°	55°
Slant Range	1100 km	1245 km
3 dB Beam Dimensions (az x el)	1.8° x 1.6°	1.7° x 1.4°
3 dB Footprint Dimensions (az x el)	34 x 44 km	37 X 52 km.
Peak Gain	38.5 dBi	39 dBi
Rotation Rate	18 rpm	
Along Track Spacing	22 km	221011
Along Scan Spacing	15 km	19 km

Table 1: SeaWinds Antenna and Measurement Geometry Parameters

Parameter	Value
Transmit Frequency	13.402 GHz
Transmit Power	110 Watts
Transmit PRF	185 Hz (92,311 z each beam)
Transmit Pulse Length	1.5 ms
Transmit Modulation	MSK, $T_b = 15\mu\text{sec}$
Receive Gate Length	2.0 111s
Receive Gate 1 Delay	7.3 ms (inner beam), 8.3 ms (outer beam)
System Noise Temperature	740°1{

Table 2: SeaWinds Radar Electronics Parameters

Wind Speed	Inner Beam		Outer Beam	
	$\sigma^0$ (dB)	$E_s$ (dBJoules)	$\sigma^0$ (dB)	$E_s$ (dBJoules)
3 m/s	-32	-184	-27	-179
8 m/s	-23	-175	-20	-172
20 m/s	-14	-167	-14	-167

Table 3: SeaWinds Expected Echo Energies

## Figure! Captions

Figure 1: SeaWinds measurement geometry.

Figure 2: SeaWinds scan pattern showing helixes traced by inner beam (light shade) and outer beam (dark shade) as spacecraft orbits. Expansion of region within box shown in Figure 3.

Figure 3: Expansion of boxed region in Figure 2 illustrating spacing of  $\sigma^0$  measurements. Measurement footprints are defined by 3 dB contour of the antenna pattern.

Figure 4: Diagram of SeaWinds electronics functions.

Figure 5: Diagram of SeaWinds filtering and detector functions.

Figure 6: Frequency domain representation of SeaWinds echo detection. Shown are the echo spectrum, white thermal noise spectrum, and the signal+noise and “noise-only” filter responses.

Figure 7: SeaWinds transmit and detection timing.

Figure 8: Example transmit spectrum ( $B_{msk} = 40$  kHz), Doppler spectrum (inner beam, scan azimuth 90 degrees), and the resultant echo energy spectrum. Also shown is an example signal+noise filter magnitude response where  $B_f = 80$  kHz.

Figure 9: (a) Percentage echo energy passed by signal+noise filter ( $\rho_E$ ) vs. filter overhead ( $B_f - B_{msk}$ ). (b) Doppler compensation error ( $\Delta_E$ ) vs. filter overhead.

Figure 10: Example of values of  $K_p$  parameters  $A$ ,  $B$ , and  $C$  vs. antenna azimuth angle.

For this case  $B_{msk} = 40$  kHz,  $B_r = 80$  kHz,  $B_n = 1$  MHz.

Figure 11:  $K_p$  vs. azimuth for different values of  $B_{msk}$ . (a) 3 m/s wind, (b) 8 m/s wind, (c) 20 m/s wind.

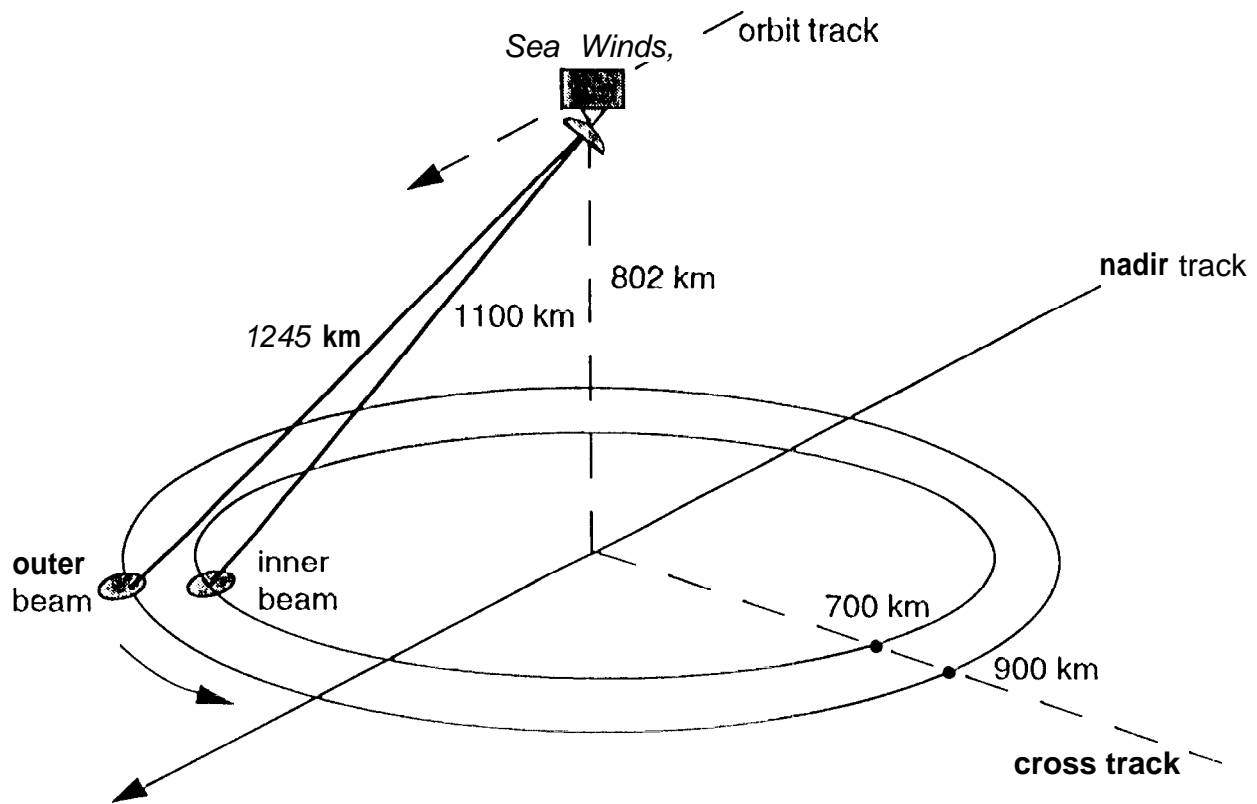


Figure 1

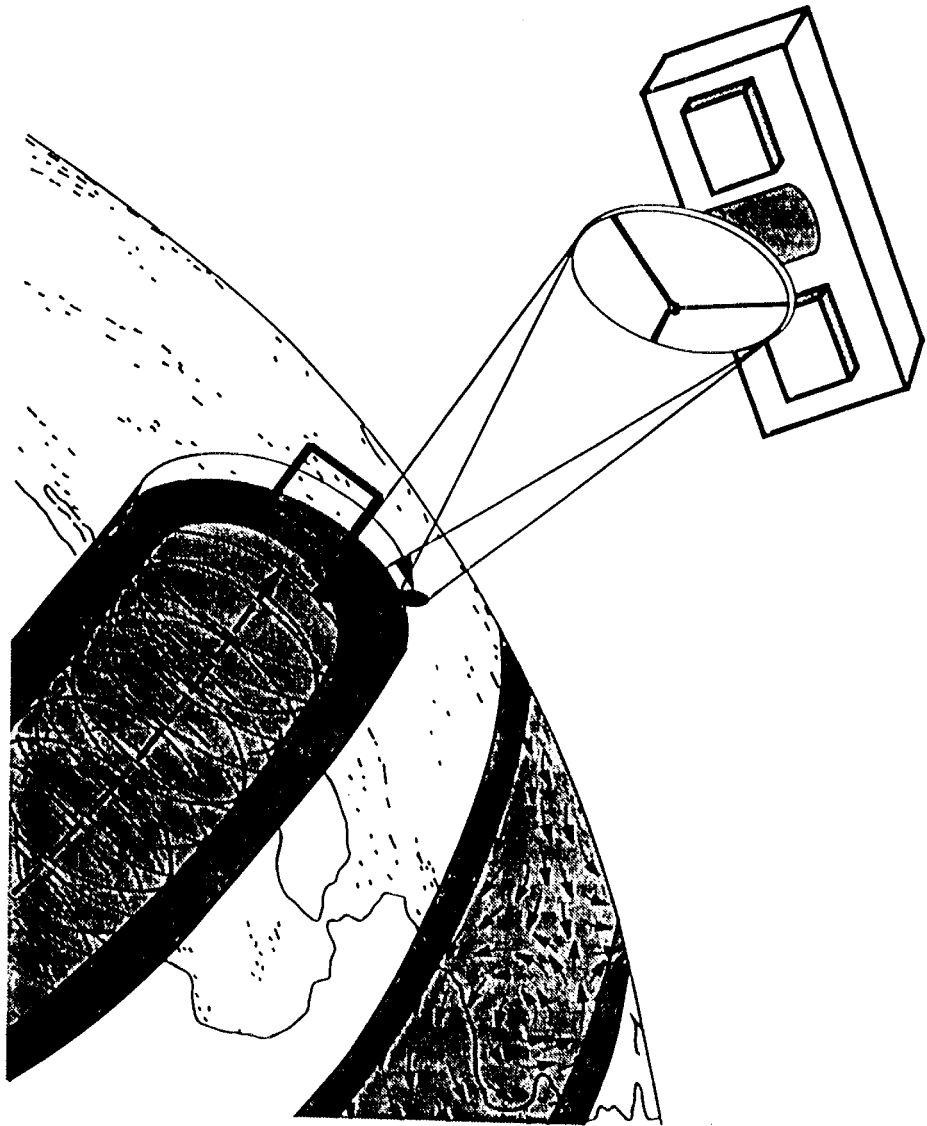


Figure 2

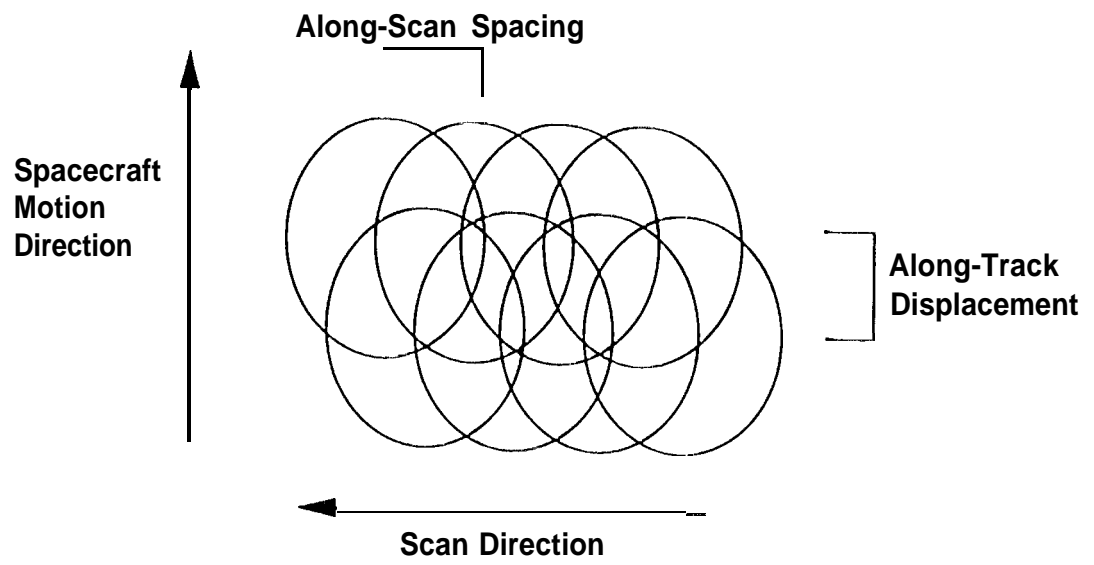


Figure 3

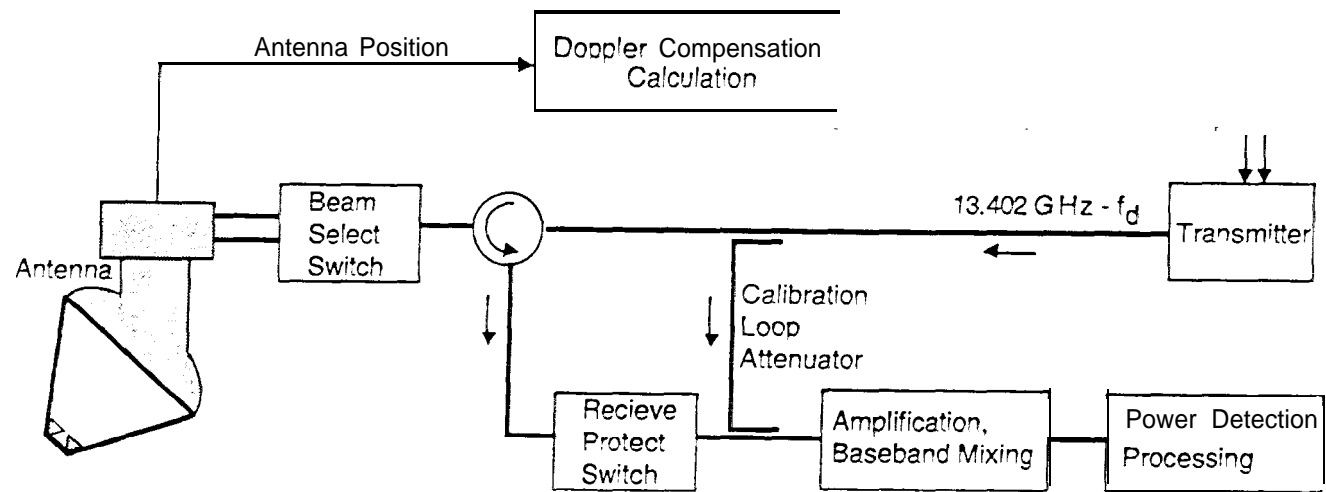


Figure 4

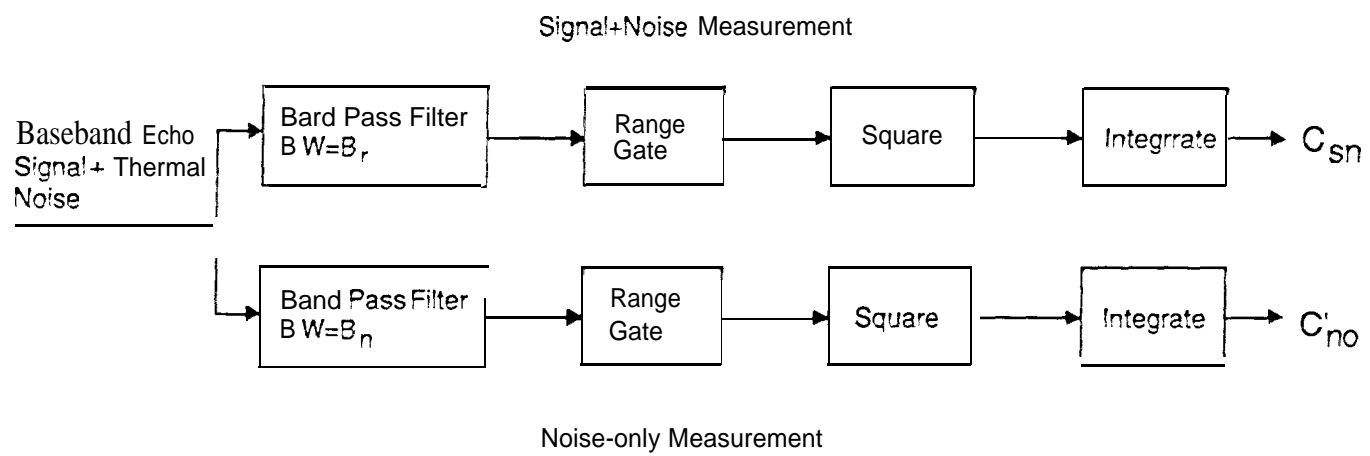


Figure 5

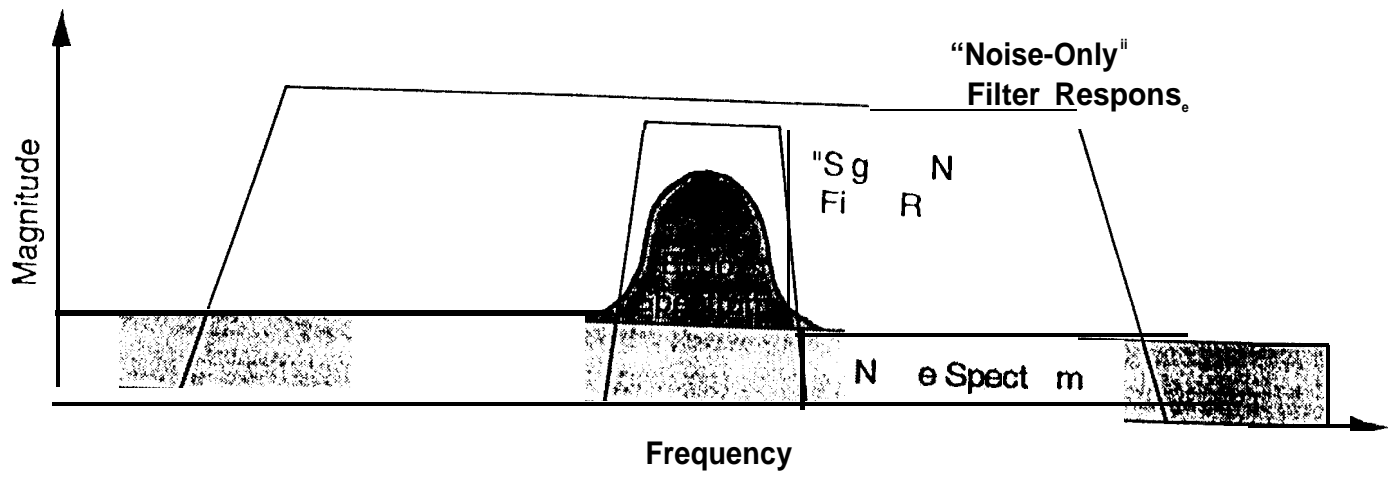


Figure 6

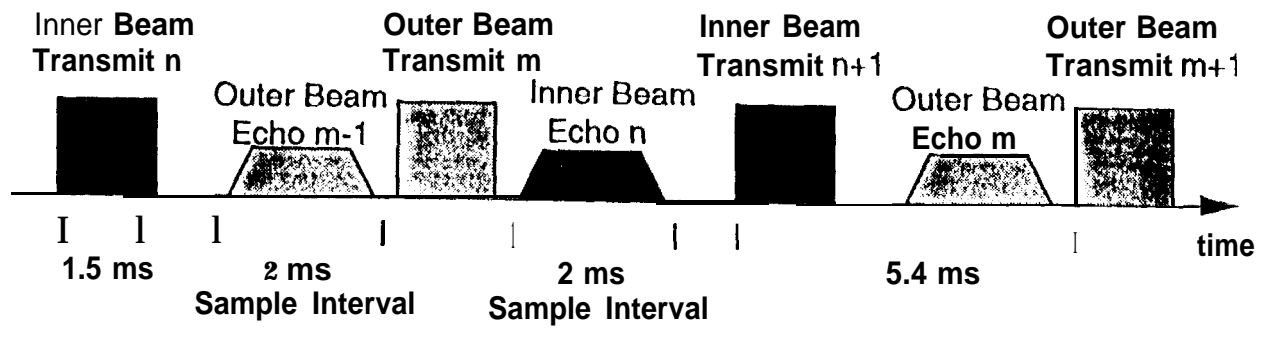


Figure 7

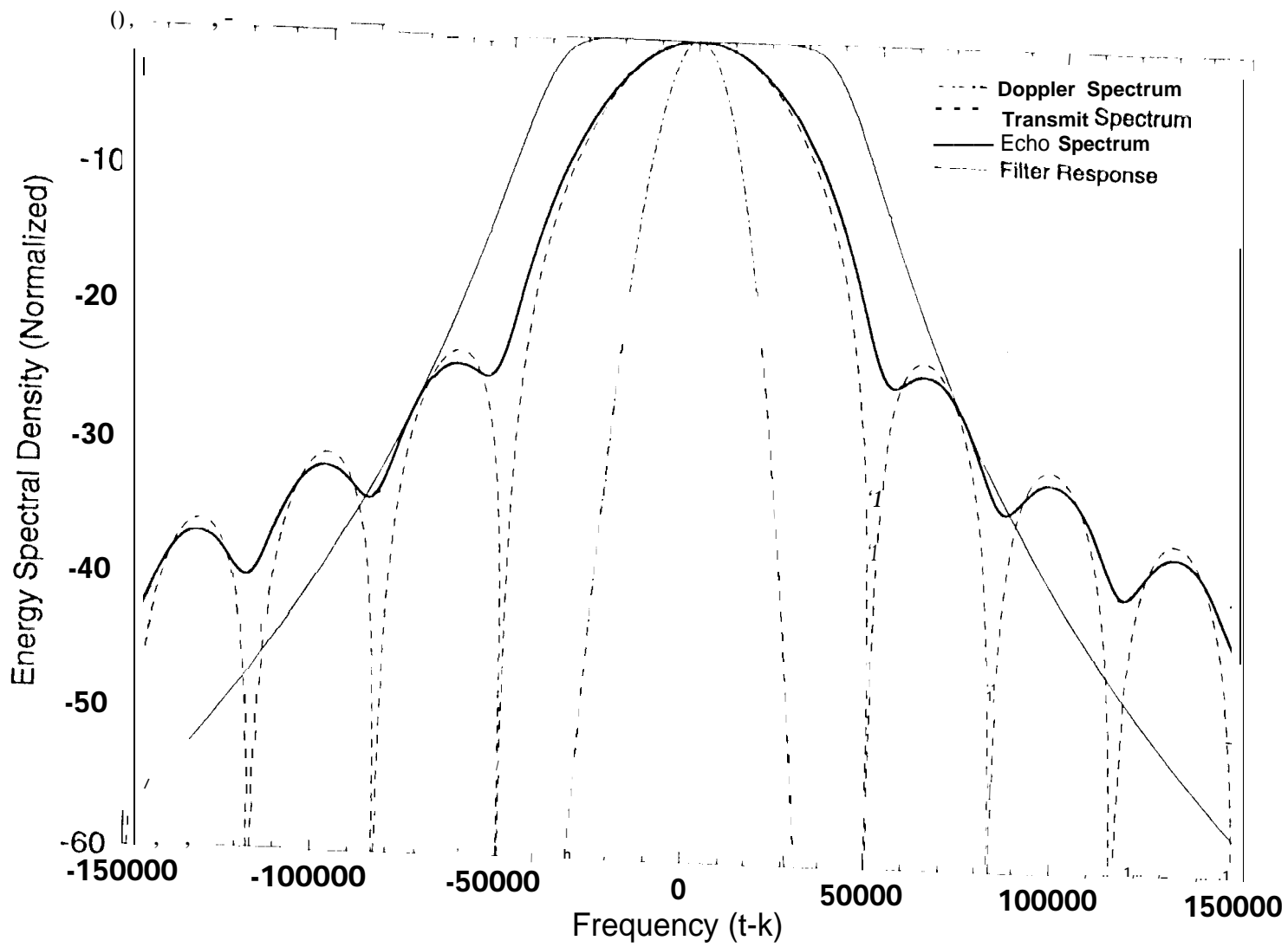


Figure 8

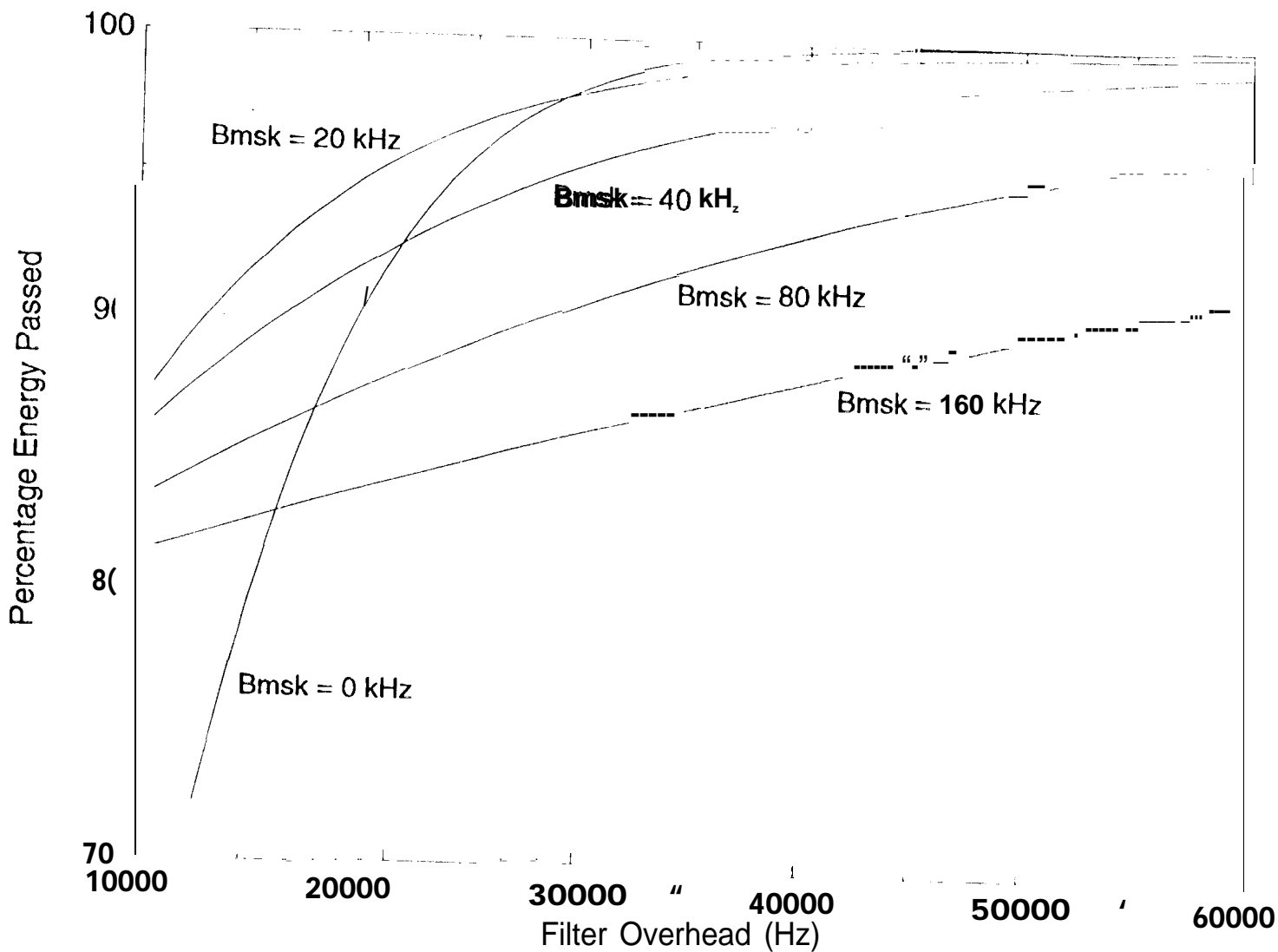


Figure 9a

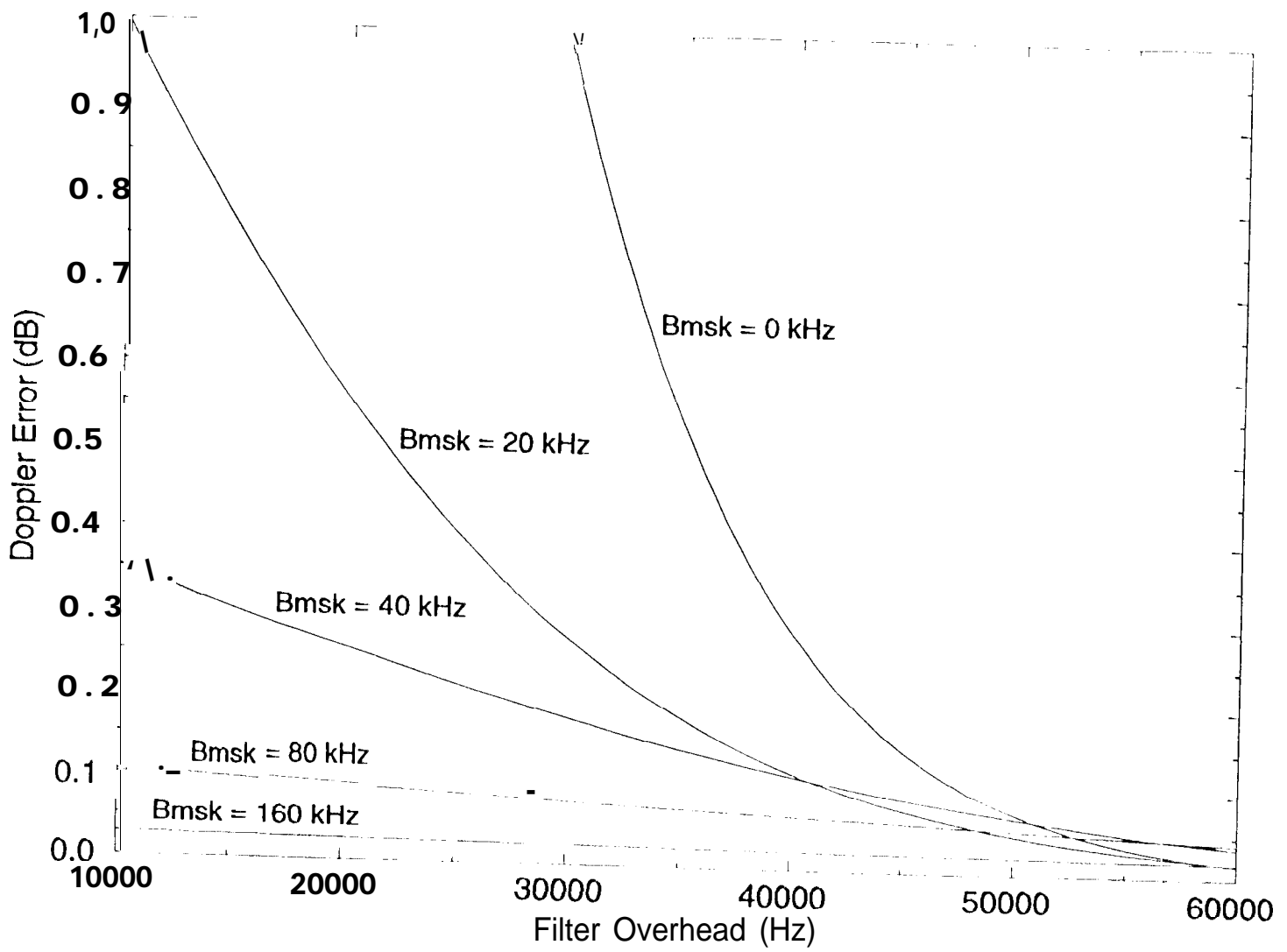


Figure 9b

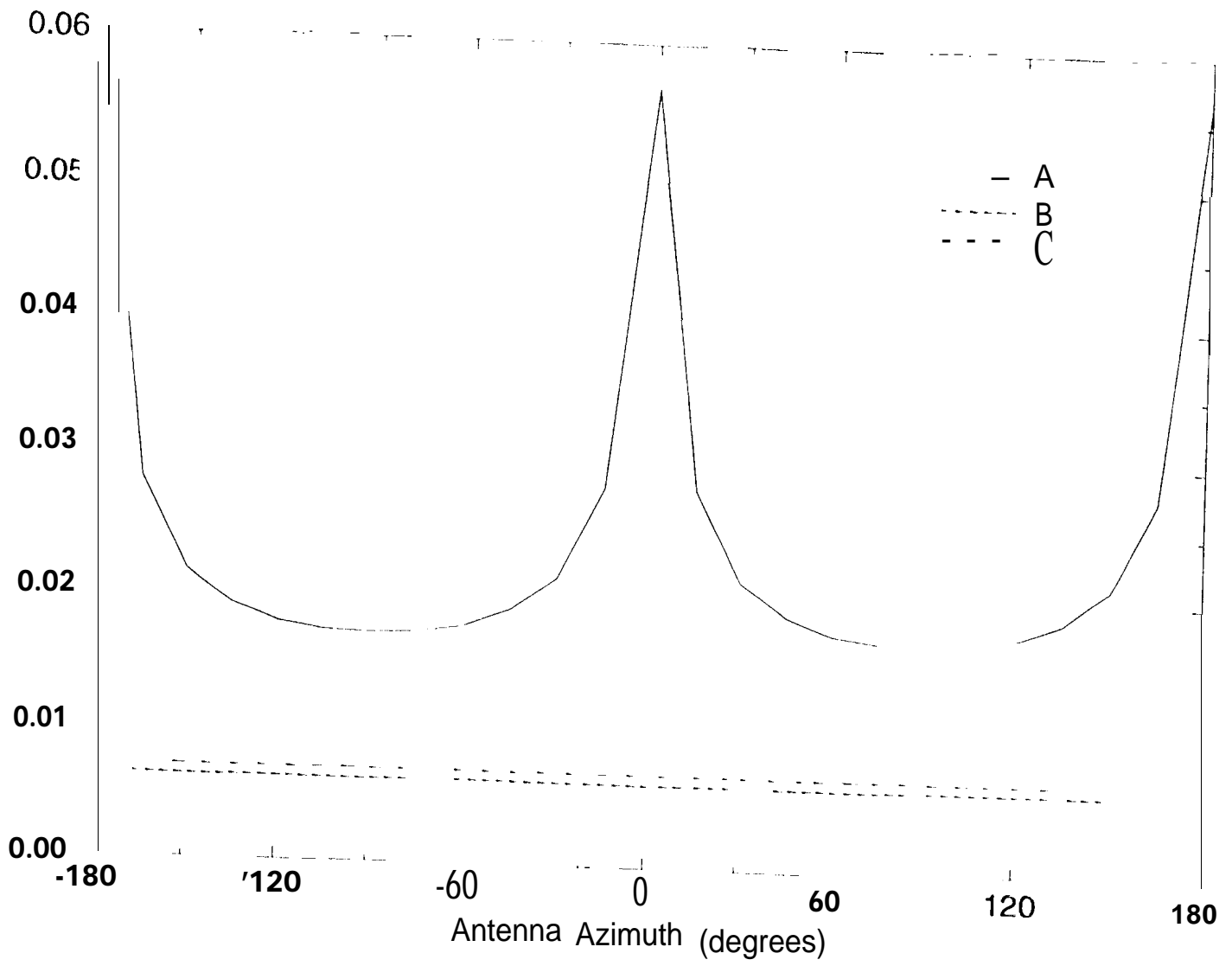


Figure 10

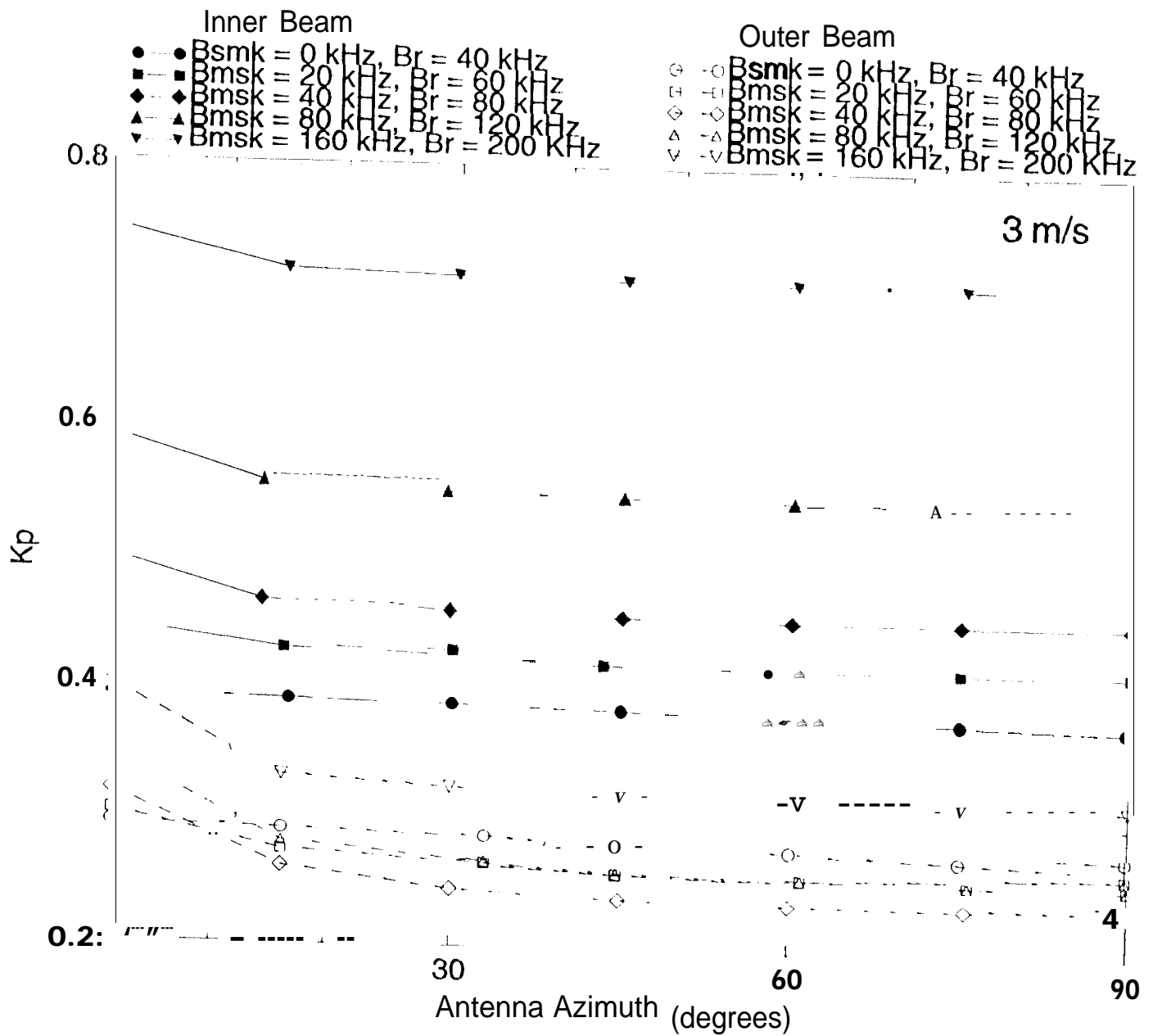


Figure 11a

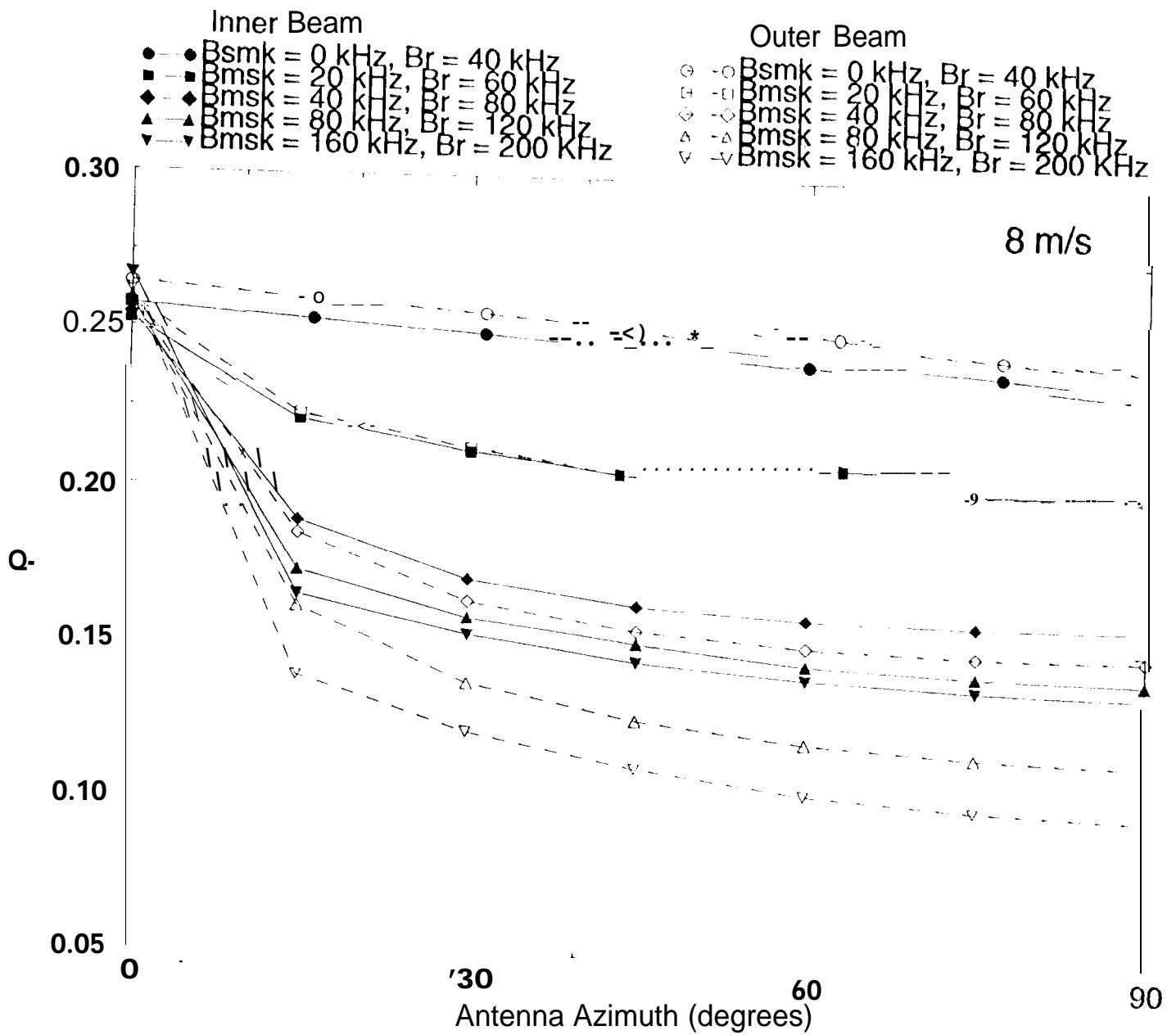


Figure 11b

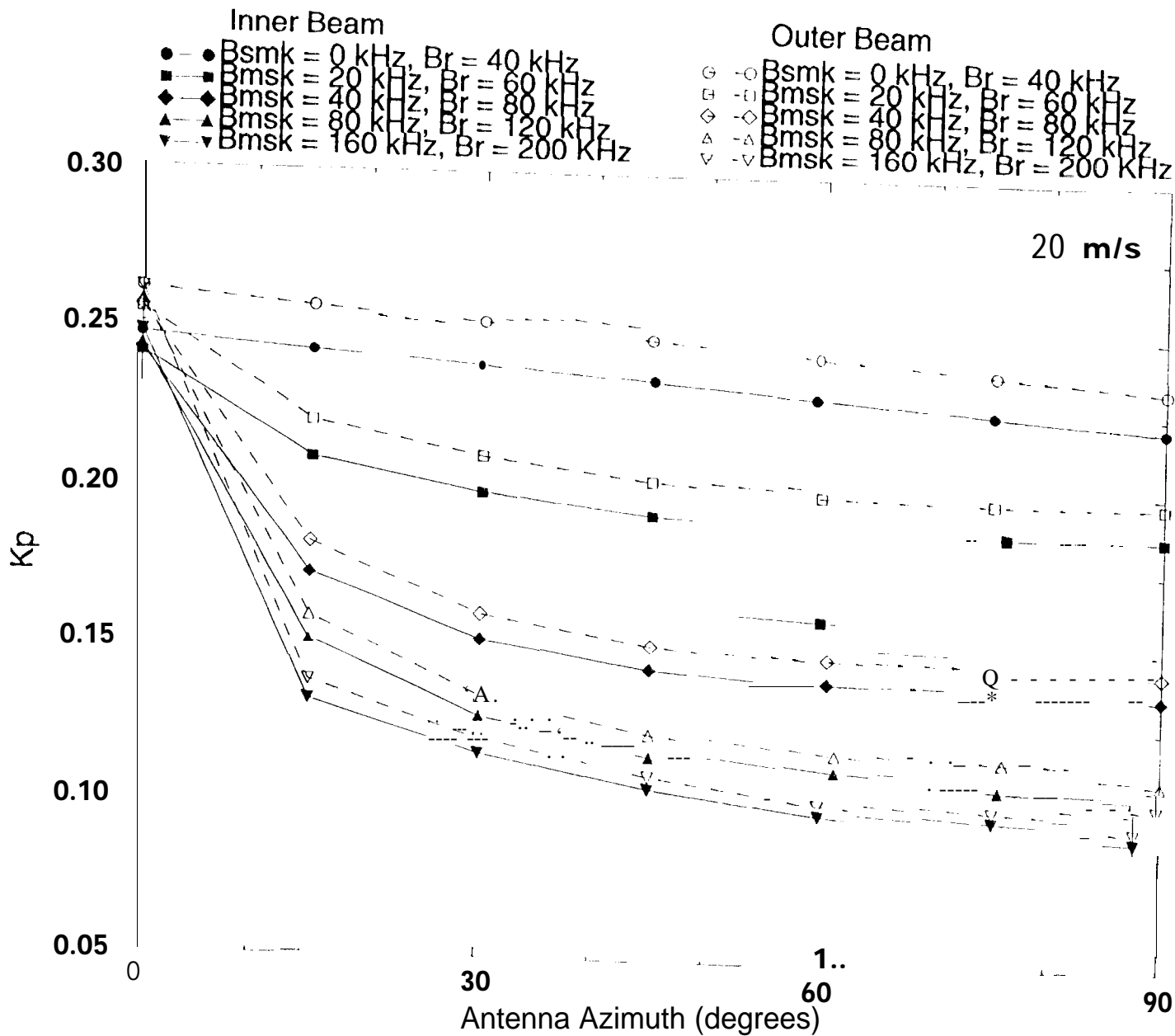


Figure 1 1c